Indications from dressed photons to macroscopic systems based on hierarchy and autonomy

M. Ohtsu

Research Origin for Dressed Photon,

3-13-19 Moriya-cho, Kanagawa-ku, Yokohama, Kanagawa 221-0022 Japan

Abstract

This article describes the size-dependent momentum resonance of the dressed photon (DP) energy transfer. The features of the hierarchy and autonomy in DP energy transfer are reviewed, together with a description of experiments carried out to confirm these features, using DP devices, nano-fabrication, and energy conversion. It is pointed out that a novel theoretical model is required to analyze these features and that the quantum-walk model is a promising theoretical tool for this analysis.

1 Introduction

A dressed photon (DP) is an off-shell quantum field created as a result of the interaction between photons and electrons (or excitons) in a nanometer-sized space [1]. The DP localizes at a nanometer-sized particle (NP) and also couples with multi-mode coherent phonons [2]. A variety of novel technologies have been developed by using the DP, including nanometer-sized optical devices, nano-fabrication technology, and highly efficient energy conversion technology [3]. Theoretical studies have been carried out to derive creation/annihilation operators and spatial localization features of the DP by modifying optical theories developed for the conventional on-shell quantum field [2]. In parallel with these theoretical studies, experimental studies have found the intrinsic features of hierarchy and autonomy in DP energy transfer. However, these features were not treated using the

theoretical studies above. The present paper reviews these features and points out that a theoretical treatment of them is necessary for realizing future progress in DP science and technology.

2 Hierarchy

As a preliminary discussion on hierarchy, this section starts by reviewing the efficiency of the DP energy transfer between the two spherical NPs (NP1 and NP2, with radii a_1 and a_2, respectively: Fig.1(a)). Theoretical studies have derived a Yukawa function that represented the magnitude of the interaction energy between the two NPs mediated by a DP [4, 5]. As a result of the interaction, propagating light was created from the NPs and could be detected by a conventional photo-detector installed in the far field. The intensity of this light is shown in Fig. 1(b) [5]. The two curves in this figure show that the efficiency resonantly takes the maximum when $a_1 = a_2$. This feature has been called size-dependent momentum resonance, which represents the momentum conservation law during the DP energy transfer.

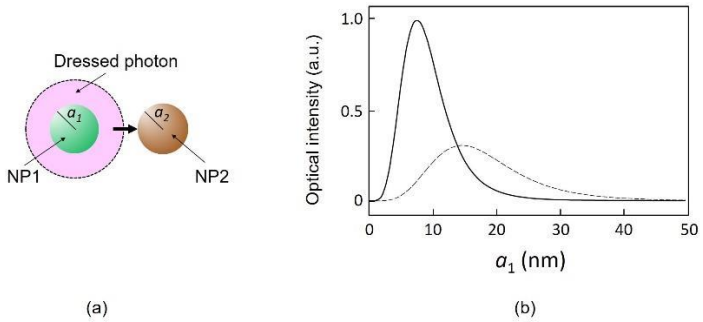

Fig. 1 Size-dependent momentum resonance.

(a) Two spherical NPs and their radii. (b) Relation between the radius and the detectable intensity of the propagating light. The solid and broken curves represent the calculated values for a_2=10 and 20 nm, respectively. The surface-to-surface separation between the two NPs is 1 nm.

This resonance feature has been confirmed by several experiments: The spatial profile of a nanometer-sized specimen was acquired by using a DP on the apex of a fiber probe as a light source in scanning probe microscopy. The contrast of the specimen's image was highest when the specimen's size was equal to the radius of curvature a of the apex of the fiber probe. In other words, the dependence of the contrast on the spatial Fourier frequency showed a band-pass feature, as shown by curve A in Fig. 2. Its center frequency was given by the inverse of the radius of curvature a. This indicated that these experiments acquired nothing more than an image of the apex of the fiber probe by utilizing the DP energy transfer to the specimen. On the other hand, as shown by curve B, the image acquired by a conventional optical microscope showed a low-pass feature whose high-frequency cutoff was given by the inverse of the wavelength λ of the light. This cutoff imposes the diffraction limit on the spatial resolution in conventional microscopy.

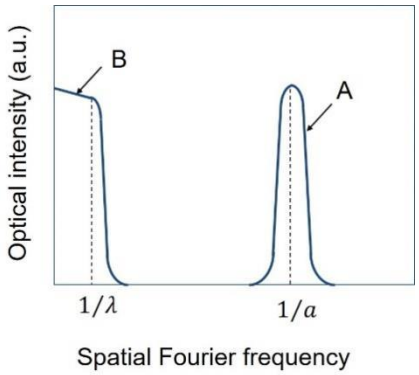

Fig. 2 Dependence of the image contrast on the spatial Fourier frequency. Curves A and B are for the images acquired by using the DP energy transfer and by a conventional optical microscope, respectively.

The bandwidth of curve A depended on the profile and size of the tapered part of the conical fiber probe. This dependence indicated that the characteristics of the acquired image also depended on the distance between the fiber probe and the specimen. In order to confirm this dependence, the

left parts of Figs. 3 (a) and (b) show images of flagellar filaments of salmonella bacteria on a glass substrate, acquired by scanning a fiber probe [6]. The probe–flagellum separations were 15 nm and 65 nm, respectively. It can be seen that the diameters of the filament-like structures in Fig. 3(a) are smaller than those in (b).

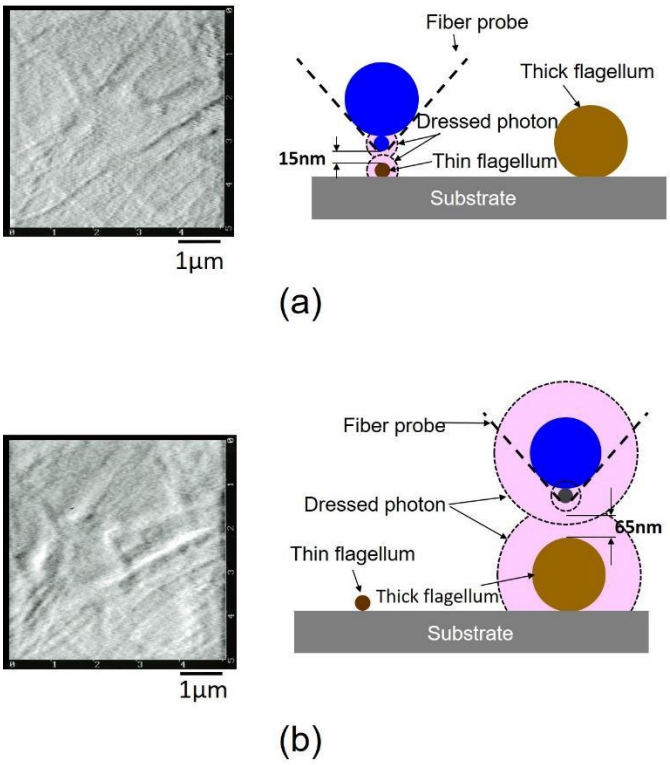

Fig. 3 Images of the flagella of salmonellae and schematic explanation of the setups used to acquire them.

(a) and (b) represent the cases with probe-flagellum separations of 15 and 65 nm, respectively.

In order to identify the origin of the difference in diameter, the right parts of Figs. 3(a) and (b) schematically show the modeled setups used to acquire these images. The probe is approximated as two blue spheres, where the smaller sphere represents the apex of the probe, and the larger sphere is placed on the smaller sphere. The pink circles in the right part of Fig. 3(a) show the DP field created on the smaller sphere and extending to the

flagellum when the probe–flagellum separation is short. This means that a high-spatial-resolution image can be acquired by the DP field on the smaller sphere due to the size-dependent momentum resonance with the flagella, even though the image is partly superposed with the low-spatial-resolution image acquired by the DP field on the larger sphere. On the other hand, as shown in the right part of Fig. 3(b), the DP field on the smaller sphere does not extend to the flagella when the probe–flagellum separation is large. Only the DP on the larger sphere extends to the flagella so as to be involved in the imaging due to the size-dependent momentum resonance, whereby a low-spatial-resolution image is acquired.

In what follows, the main discussions on hierarchy can be started based on the size-dependent momentum resonance described above. Here, it is assumed that two spherical NPs (NP1 and NP2 with radii a_1 and a_2, respectively) are installed in close proximity to each other (Fig. 4). It is also assumed that two more NPs (NP1' and NP2', with radii $a_1^{'}(>a_1)$ and $a_2^{'}(>a_2)$, respectively) are installed in proximity to NP1 and NP2. The size-dependent momentum resonance realizes efficient energy transfer of the DP on NP1 to NP2 when $a_1 = a_2$. Although the energy on NP1' is also efficiently transferred to NP2' when $a_1^{'} = a_2^{'}$, the efficiency of the transfer to NP2 is low due to the size difference ($a_2 \neq a_2^{'}$). The efficiency of the transfer from NP1 to NP2' is also low. That is, the channels of the DP energy transfer between the different-sized pairs do not exhibit any crosstalk. This feature of DP energy transfer without any crosstalk is called *hierarchy* in this article. It means that different energy transfers occur independently for different material sizes. A hierarchical memory has been developed by using this hierarchy feature [7].

For further discussions on hierarchy, one should consider the "size" of the material. In the case of a spherical NP, its size is represented by its radius. However, even though it is recognized as a sphere when it is viewed in the far field, its surface often has roughness when it is viewed in the near

field. That is, the recognized shape and size depend on the separation between the NP and the observer. The hierarchy is related to these separation-dependencies. If the surface of the above-mentioned spherical NP is divided into small parts, and they are approximated as spheres whose radii are equivalent to the size of the roughness, discussions equivalent to those of the original spherical NP can be made. The concept of hierarchy is established by assuming that the spatial features of the divided parts are equivalent to those of the original spherical NP.

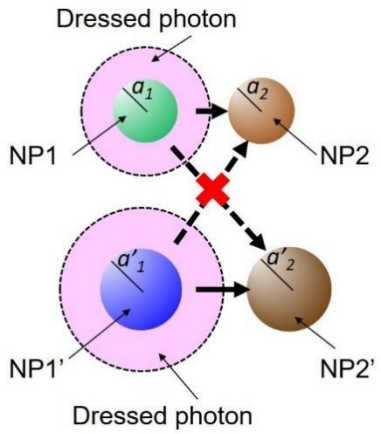

Fig. 4 Schematic explanation of hierarchy.

However, this division cannot be repeated infinitely. The minimum size of the NP to be divided obviously corresponds to the size of an atom, for which the discussions of hierarchy above are valid. On the other hand, experimental studies have estimated that the maximum size of the DP was 50-70 nm [8], which corresponds to the maximum size of the NP for which discussions of hierarchy are valid.

3 Autonomy

Experiments have observed unique characteristics of the DP energy transfer among NPs. From these characteristics, it appears as if DP energy transfer occurs of its own will, and thus this behavior has been called autonomy [2].

The origins of this autonomy have been attributed to the size-dependent momentum resonance and hierarchy. Furthermore, based on this autonomous behavior, the DP behaves like an organism. That is, the DP seems to indicate two things of its own will. They are:

{1} *The DP indicates its existence to the macroscopic system most effectively.*

The experimental ground for this indication is:

The DP in the nanometer-sized system autonomously selects the route for transferring its energy so as to maximize the power of the generated propagating light (the output signal) [Section 3.1].

{2} *The DP indicates that it minimizes the magnitude of the energy dissipation of the macroscopic system by removing the DP energy from the nanometer-sized system most effectively.*

The experimental grounds for this indication are:

- The DP autonomously annihilates so as to minimize the energy dissipation of incident light during the process of etching a bump on a material surface [Section 3.2].
- The DP autonomously modifies the spatial distribution of B atoms so as to maximize the emitted light power whose photon energy is equivalent to that of light irradiated during the device fabrication* (photon breeding**) [Section 3.3].
- The DP autonomously modifies the spatial distribution of Ag particles so as to maximize the output photocurrent when the input light has the same photon energy as that of the light irradiated during the device fabrication* (photon breeding**) [Section 3.4].

(*) Sections 3.3 and 3.4 reveal that the spatial distributions of the B and Ag atoms, respectively, were controlled by the DP. Furthermore, these atoms form pairs, and these pairs induce photon breeding. This induction is analogous to the induction of the self-duplicating function originating from the pair of helices in DNA.

(**) The photon breeding indicates that the light emitted from the device is a replica of the light irradiated on the crystal during the device fabrication. That is, the emitted light is self-duplicated by the irradiated light, which suggests that the behavior of the DP is analogous to that of organisms.

3.1 DP devices

DP devices are novel nanometer-sized optical devices that control and transmit an optical signal by using the DP energy transfer among NPs [2].

Figure 5 shows the basic structure of a DP energy transmitter, which is a representative example of a DP device. It is composed of an array of N NPs of the same size (NP_1 – NP_N), and one large NP (NP_O). They are arranged accurately with a constant separation. In the case of using cubic semiconductor NPs, an exciton is created in energy level $(1,1,1)$ of NP_1 by applying an input signal, i.e., by irradiating NP_1 with propagating light. This exciton creates a DP. The created DP is transferred toward NP_N, and nutation occurs among the N NPs. As a result, these NPs are coupled with each other. If the size of NP_O is adjusted so that its electric dipole-forbidden level $(2,1,1)$ is resonant with the energy level of the coupled state of the N NPs, nutating energy is transferred to NP_O so as to create an exciton in the energy level $(2,1,1)$ of the NP_O. By subsequent relaxation of the exciton to the lower energy level $(1,1,1)$ of the NP_O, the light is emitted from the exciton in energy level (1,1,1) and is used as the output signal. It should be pointed out that this relaxation (in other words, energy dissipation) is essential for generating the output signal.

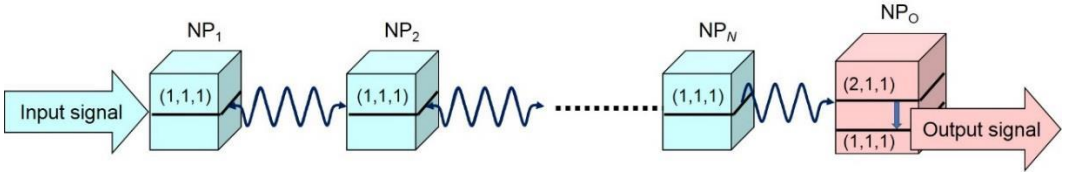

Fig. 5 Structure of energy transmitter.

For device fabrication, it is much easier to randomly disperse NP_1 – NP_N and NP_O on a substrate than to accurately arrange them with a constant separation. Figure 6(a) schematically explains such a configuration [9], in which small NPs are randomly dispersed along the x-, y-, and z-axes, and are used as NP_1 – NP_N (the numbers of rows are denoted by N_x, N_y, and N_z, respectively). NP_O is installed among the small NPs. NP_1 and NP_O in Fig. 5 are respectively denoted by NP_{in} and NP_{out} in this figure.

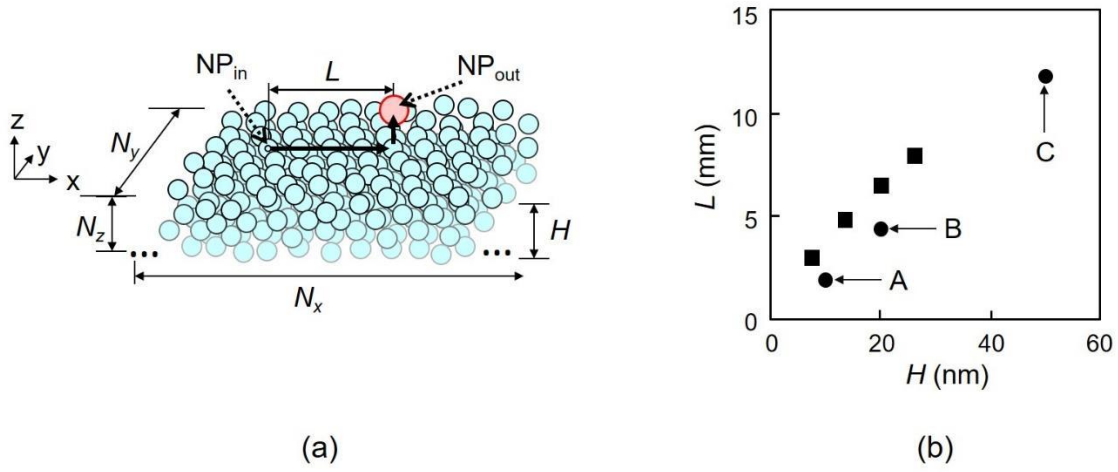

Fig. 6 Calculated results for NPs dispersed on a planar substrate.

(a) Arrangement of multiple small NP (NP_S) and one larger NP (NP_L).

(b) Dependence of the energy transmission length L on the thickness H of the small NP layers. Closed circles show the measured values for the devices A, B, and C. Closed squares are calculated values.

CdSe NPs were used for experimental confirmation of the device operation. Although they have spherical shapes, a discussion of the cubic NPs in Fig. 5 is valid. The diameters of NP_1 – NP_N were maintained at 2.8 nm, whereas that of NP_O was 4.1 nm in order to satisfy the resonance condition between the exciton energy levels (1,1,1) and (2,1,1) in Fig. 5. These NPs were dispersed on a SiO_2 substrate, and the average separation

between the adjacent NPs was arranged to be 7.3 nm in order allow efficient DP energy transfer. Moreover, the thickness of the NP layers, H in Fig. 6(a), was fixed to 10 nm, 20 nm, and 50 nm, which are proportional to the number of rows N_z of NP_1 – NP_N along the z-axis. These devices are denoted by A, B, and C, respectively.

The NP_{in} were illuminated with propagating light of 473 nm-wavelength, and the energy transmission length L was measured as a function of H. The results are shown by closed circles in Fig. 6(b), from which the values of L for devices A, B, and C were found to be 1.92 μm, 4.40 μm, and 11.8 μm, respectively. These are much longer than the wavelength of the incident light, confirming that the transmission loss was low. These results show that the DP energy was transferred autonomously among the NPs even though they were randomly arranged. This figure shows that the measured values agree with the values (closed squares in this figure) calculated by using the phenomenological rate equations. It also shows that L increases with increasing H, i.e., with increasing N_z. This autonomous signal transmission has been reproduced by a simulation based on quantum master equations for the density matrices [10].

It has been found that this autonomous DP energy transfer showed the following two characteristics [11], suggesting that there exists an optimum arrangement of the NPs that give indication {1} above.

[Characteristic 1] *The efficiency in energy transfer is highest when* $N \cong 4$: The DP energy transfer from multiple NP_S to one NP_L has been analyzed [12]. As is schematically explained by Fig. 7(a), the device under analysis contained N small NPs (NP_S) and one large NP (NP_L). By assuming that each NP_S was initially occupied by an exciton, quantum master equations for the density matrices were solved to derive the occupation probability of the exciton in energy level (1,1,1) of NP_L. The time-integrated value of this probability is proportional to the output signal intensity. This intensity was calculated as a function of the number N of CdSe NP_S. The calculated

results are indicated by closed circles in Fig. 7(b) and show that the efficiency of energy transfer was highest when $N \cong 4$. Since the radiative relaxation rate from the lower energy level of NP_L took a finite value, the DP energy was not transferred to NP_L until the exciton in energy level (1,1,1) was annihilated, and as a result, the energy was dissipated from NP_S if N was too large. Therefore, the output signal intensity did not increase if too many NP_S were installed around an NP_L, which meant that the efficiency of the energy transfer to NP_L decreased when $N > 4$. Small and large spherical CdSe NPs (2.0 nm and 2.8 nm diameters, respectively) were used to experimentally measure the magnitude of the energy transferred from NP_S to NP_L [13]. The results are represented by the closed squares in Fig. 7(b). They show that the output signal intensity was highest at $N \cong 4$, in agreement with the calculated results.

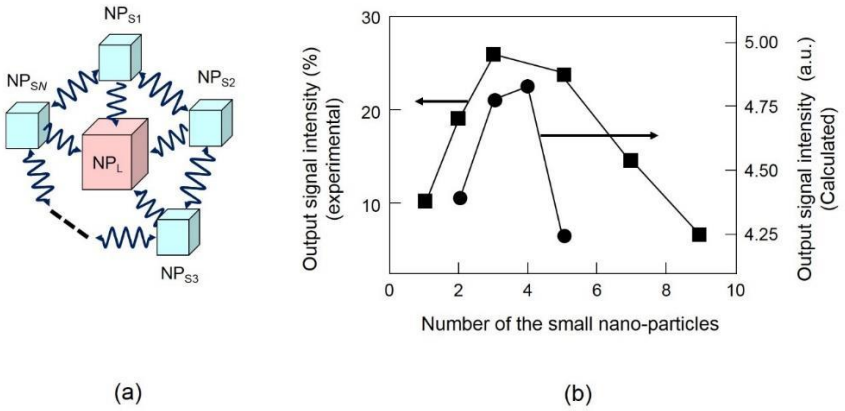

Fig. 7 Autonomy of the DP energy transfer.

(a) Layout of NPs. (b) Dependences of the output signal intensities emitted from CdSe NP on the ratio of the number of NP_Ss to that of NP_L.

[Characteristic 2] *If the interaction between one of the NP_S and NP_L is degraded or lost, the DP energy at this NP_S does not transfer to the other NP_S but is efficiently stored in this NP_S until the DP energy is transferred to NP_L. This efficient storage indicates that the transferred energy*

autonomously searches for unoccupied NPSs in the system: Let us assume that the interaction between some NP_S and NP_L may be degraded or lost because of size-detuning of the NPs, fluctuations in the separations between the NPs, or deterioration of the NP materials. In the case of a pentagonal layout, as shown in Fig. 8(a), there can be seven degraded configurations: By referring to system E0 as the one without any degradation, system E1 represents the layout in which the interaction between one NP_S and NP_L is degraded or lost (represented by the red mark × between NP_{S1} and NP_L in this figure). Systems E2 and E2' have two degraded interactions. Figure 8(b) shows the time-integrated values of the occupation probability of the exciton in NP_L for the eight systems (E0–E5). This figure shows that system E5 does not generate any output signals because the interaction between NP_S and NP_L is completely lost. In contrast, the output signal intensities from systems E1–E4 with degraded interactions are larger than that from system E0. In particular, the value of the output signal intensity from system E2 is 1.64-times larger than that from system E0. Moreover, the autonomy in the DP energy transfer can be understood from Fig. 8(c). This figure shows the temporal evolutions of the occupation probabilities of excitons in the energy levels of five NP_S in system E2, in which two interactions are degraded (NP_{S2}–NP_L and NP_{S3}–NP_L). The energy levels in all the NP_Ss are initially occupied by excitons, and afterward for several nanoseconds, the occupation probabilities in NP_{S2} and NP_{S3} remain high, which means that the DP energy does not transfer to the other NP_Ss but is efficiently stored in this NP_S until the DP energy is transferred to NP_L. On the other hand, Fig. 8(d) shows the time evolutions of the occupation probabilities in the case of system E0, in which the energy levels of three NP_Ss (NP_{S1}, NP_{S3}, and NP_{S4}) are initially occupied by excitons. It is found from this figure that the occupation probabilities for NP_{S2} and NP_{S5} increased within 2 ns even though they were initially zero. This means that the transferred DP energy autonomously searches for unoccupied NP_Ss in the system.

Characteristics 1 and 2 originating from the autonomy in the DP energy transfer can be applied to novel information technologies: Since the phenomenon of autonomous DP energy transfer between NMs is similar to the inherent behaviors of amoeba used for bio-computing [14], several simulations have been carried out for applying this phenomenon to novel non-von Neumann type computing systems in order to solve constraint satisfaction problems, Boolean satisfiability problems, and decision making problems [15].

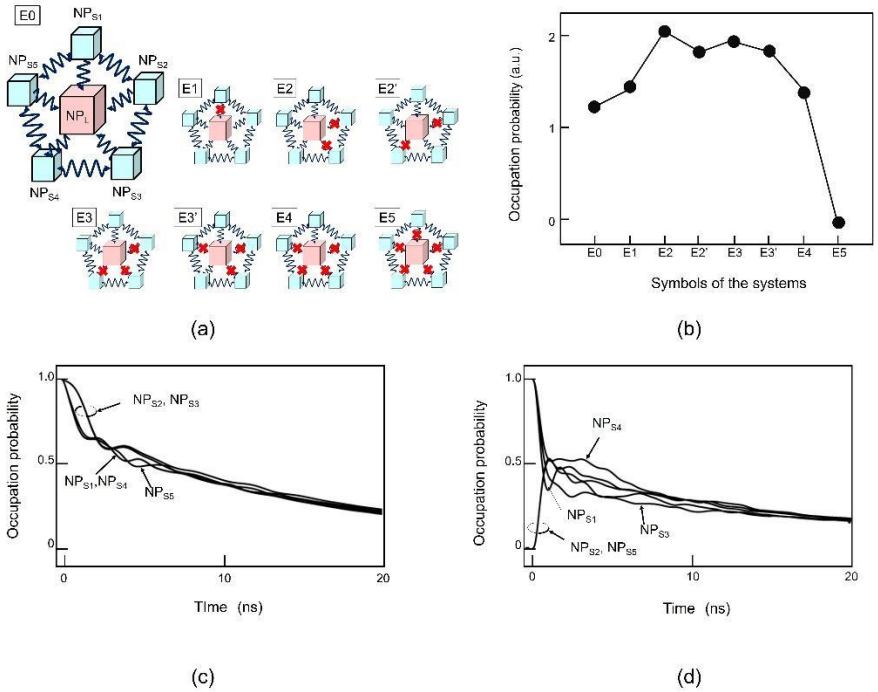

Fig. 8 Degraded or lost interaction between NP_S and NP_L.

(a) Layout of the NPs. (b) Time-integrated values of the occupation probabilities for systems E0 to E5. (c), (d) Temporal evolutions of the occupation probabilities of the exciton in the energy levels in five NP_Ss in systems E2 and E0, respectively.

3.2 Nano-fabrication technology

This section reviews a method of smoothing a material surface as an example of nano-fabrication technology using the autonomous DP energy transfer [16]. The material to be smoothed is placed in a vacuum chamber, and the

chamber is filled with a molecular gas. As shown in Fig. 9(a), the DP is created at the apex of a bump on the material surface when it is irradiated with light*. The molecule can be dissociated if it jumps into the field of this DP (Fig. 9(b)). The chemically active and radical atom created as a result of this dissociation etches the apex of the bump away. For this etching, the photon energy of the irradiated light is tuned to be lower than the excitation energy of the molecules. Even with such low photon energy, the DP efficiently dissociates the molecule with the help of the energies of phonons that are the constituent elements of the DP. It should be noted that the molecules are not dissociated by propagating light having such a low photon energy. As a result, the bump on the surface is selectively etched away.

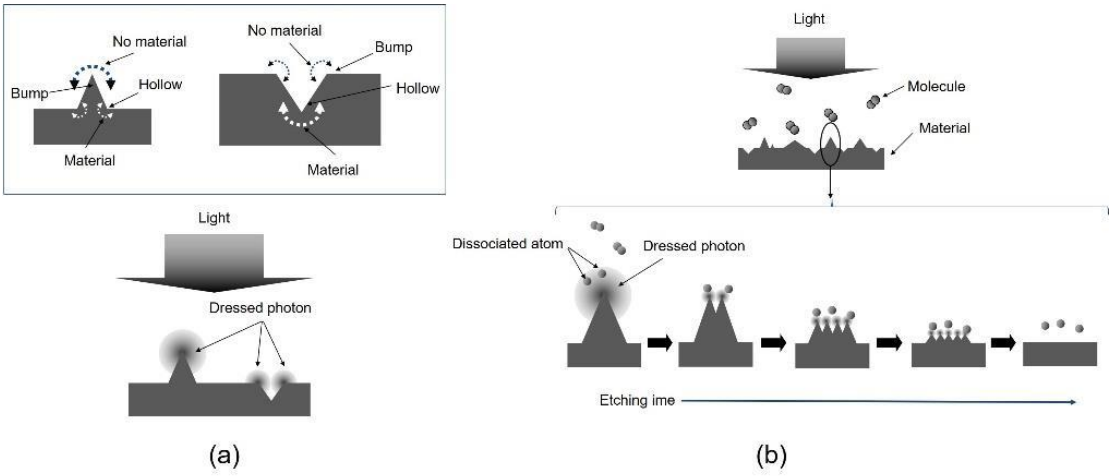

Fig. 9 Principle of chemical etching using DP for smoothing a material surface. (a) Creation of the DP at the apex of a bump. (b) Temporal variations of the surface profile as autonomous etching proceeds.

(*) It should be noted that the DP is not created at the bottom of the hollow in the surface. This is because, as shown in the square of Fig. 9(a), the bottom of the hollow is surrounded by a “macroscopic” material. The DP is always created and localized on a “nanometer-sized” material.

The closed squares in Fig. 10 represent the values of the surface roughness of a planar synthetic silica substrate, obtained from an atomic force microscope image. Gaseous Cl_2 molecules were used for etching. The wavelength of the irradiated light was 532 nm, and thus, the corresponding photon energy (2.33 eV) was lower than the excitation energy E_{ex} (=3.10 eV) of Cl_2. However, as was explained above, the DP efficiently dissociated the Cl_2 molecule, and the bump on the surface was selectively etched away.

The dotted curve in this figure shows the scattered light intensity of supplementary laser light which illuminated the substrate surface to monitor the surface roughness as etching proceeded. Its photon energy (wavelength: 632 nm) was set sufficiently lower than E_{ex} so as to neglect its contribution to the selective etching [17]. The temporal evolution feature of this scattered light intensity, monitored in real-time, was equivalent to that represented by the closed squares. This figure shows that the roughness and the scattered light intensity temporarily increased at around 10 min after the etching started. From spatial power spectral density analysis of the surface profiles, it was confirmed that these temporary increases occurred because a single tall bump was autonomously split into several lower bumps by the etching, as is schematically explained by Fig. 9(b). However, as etching proceeded further, the roughness decreased gradually.

Selective etching of the bump was spontaneously started by light illumination. The etching progressed autonomously to decrease the roughness so as to decrease the scattering of the two light beams that were used for creating the DP and for real-time monitoring, respectively. The etching spontaneously stopped when DPs were not created any more. In other words, the DPs were autonomously annihilated so as minimize the time-integrated magnitude of the energy of the scattered light. This magnitude corresponded to that of the energy dissipation of the incident light for creating the DP, and this autonomous annihilation corresponds to indication {2} above.

Smoothing of not only a planar synthetic silica substrate, but also substrate surfaces with a variety of shapes and materials has been performed. Details of this technology have been reviewed in [2].

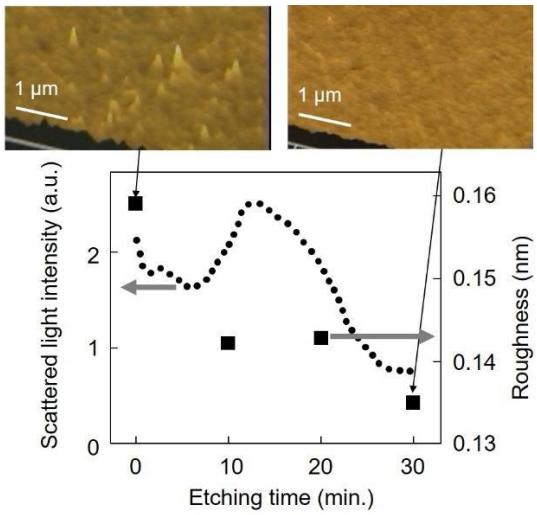

Fig. 10 Experimental results of smoothing the surface of a synthetic silica substrate. The two upper figures are atomic force microscope images of the surface. The closed squares represent the value of the roughness. The dotted curve represents the scattered light intensity.

3.3 Conversion from electrical to optical energy

This section reviews light-emitting diodes (LEDs) fabricated by using crystalline silicon (Si) as an example of converting electrical energy to optical energy. First, it should be noted that Si has been considered as being unsuitable for light-emitting devices because it is an indirect-transition type semiconductor: Because the bottom of the conduction band and the top of the valence band in Si are at different positions in reciprocal lattice space, the momentum conservation law requires an interaction between an electron–hole pair and phonons for radiative recombination. However, the probability of this interaction is extremely low.

Drastic increases of this probability have been recently realized by

using the DP for fabricating and operating devices, as explained below. As a result, a high-power Si-LED has been realized [18]. For this fabrication, the autonomous DP energy transfer was used.

[Fabrication] A novel fabrication method, named DP-assisted annealing, has been invented [19]. Joule energy was generated by injecting a forward current into a pn-homojunction in a Si substrate. It heated the substrate to diffuse p-type dopant boron (B) atoms. During this heating, the substrate surface was illuminated with light to create DPs at the B atoms. The created DPs were localized at the B atoms and coupled with localized phonons. Since these phonons provided their momenta to the electrons in the conduction band, radiative recombination between the electrons and positive holes occurred, emitting photons. Since the emitted photon energy was dissipated out from the crystal, local cooling occurred in the region where the photons are emitted. By the balance between this local cooling and the Joule-heating described above, the diffusion rate of the B atoms was autonomously controlled, and finally, the spatial distribution of B atoms reached a stationary state. Experimental studies have found that two B atoms were apt to form a pair in the stationary state, and its length d was 3-times that of the lattice constant a of the Si crystal ($d = 3a$). Furthermore, the orientation of the pair was apt to be perpendicular to the propagation direction of the irradiated light. A recent experimental study has confirmed that B atom pairs were apt to form a chain-like configuration [18].

[Operation] The light irradiated during the fabrication was not required for operating the fabricated LED device. By a simple forward current injection, as was the case for conventional LEDs, electrons were injected into the conduction band in the pn-homojunction. As a result, the electrons created a few photons by spontaneous emission even though the probability was extremely low. Once the photons were created, they created DPs that were localized at the B atoms and coupled with phonons. These DPs interacted with the electrons and provided the phonon momenta to these electrons,

allowing recombination between the electrons and positive holes, and emitting secondary photons. By repeating the provision of the phonon momenta and photon emission, the emitted light intensity increased and reached a stationary state within a short time, resulting in stable high-power photon emission. Because $d = 3a$, the electron received momenta from three localized optical phonons that were created at the B atom-pair and coupled with the DP. Therefore, the photon energy $h\nu_{em}$ of the emitted light was expressed as $h\nu_{em} = E_g - 3E_{phonon}$, where E_g and E_{phonon} are the bandgap energy of Si and the energy of the localized optical phonon, respectively. By substituting the numerical values into this equation, it was confirmed that the value of $h\nu_{em}$ was equal to that of the photon energy $h\nu_{anneal}$ of the light irradiated during the DP-assisted annealing. The phenomenon in which $h\nu_{em}$ is equal to $h\nu_{anneal}$ has been called photon breeding. This corresponds to indication {2} above.

It is widely known that the light emitted from conventional LEDs is unpolarized. However, the light emitted from an LED fabricated by DP-assisted annealing was polarized [20]. This was because photon breeding occurred not only for the photon energy but also for the photon spin. For example, by radiating light with linear polarization along the *x*-axis during the DP-assisted annealing, the B atom-pairs were apt to orient along the *y*-axis due to the autonomous control of the spatial distribution of B atoms. This DP-assisted annealing succeeded in fabricating an LED that emitted light linearly polarized along the *x*-axis, as was the polarization of the light irradiated during the fabrication process.

By applying DP-assisted annealing for autonomously controlling the spatial distribution of the p-dopant atoms, a variety of light-emitting devices have been fabricated in addition to the Si-LEDs described above. The first example is Si-lasers [21]. The second is LEDs using SiC crystals even though they are a typical indirect-transition type semiconductor, as was the case for

the Si crystal [22]. Furthermore, a novel polarization-rotation device has been developed by modifying the electrode structures of the SiC-LED above [23]. This novel magneto-optical device indicated that the SiC crystal acquired a ferromagnetic property as a result of the autonomous control of the spatial distribution of p-type dopant Al atoms by DP-assisted annealing.

3.4 Conversion from optical to electrical energy

This section reviews photovoltaic devices fabricated and operated by using organic P3HT films as an example of devices that convert optical energy to electrical energy [24]. Indication {2} above is involved here.

[Fabrication] A P3HT film was used as a p-type semiconductor, and a ZnO film was used for an n-type semiconductor, as is schematically explained in Fig. 11(a). The principal properties of the device depended on the P3HT film because the depletion layer in the pn-heterojunction was formed in the P3HT film. A transparent ITO film and Ag film were used as electrodes, resulting in a cross-sectional structure shown in the upper-left of this figure. Ag particles were deposited on the Ag film by rf-sputtering, during which the surface of the Ag film was irradiated with light and a reverse voltage V_b was applied to the pn-heterojunction. Here, the wavelength λ_0 of the irradiated light was set longer than the cutoff wavelength λ_c, which corresponds to the inverse of the bandgap energy E_g of the P3HT film. DPs were created at bumps of the surface of the Ag film, as was the case of Fig.9. As a result, the amount of Ag particles that flowed into and out of the Ag film surface was autonomously controlled by these DPs. This control process is summarized as follows: (1) the generation of electron-hole pairs by the DP (Part (1) in Fig. 11(a)), (2) charging the Al film (Part (2) in Fig. 11(a)), and (3) autonomous control of Ag particle deposition (Part (3) in Fig. 11(a)). By processes (1)-(3), a unique surface morphology was formed on the Ag film,

which was governed by the spatial distribution of the DPs.

[Operation] By radiating light for operating the fabricated device, DPs were created efficiently on the Ag electrode surface (Fig. 11(b)). Electron-hole pairs were created in the pn-heterojunction by the help of the phonon energy in these DPs even though the photon energy of the incident light was lower than E_g. This indicated up-conversion of optical energy to electrical energy. As a result, conversion from optical energy to electrical energy was realized.

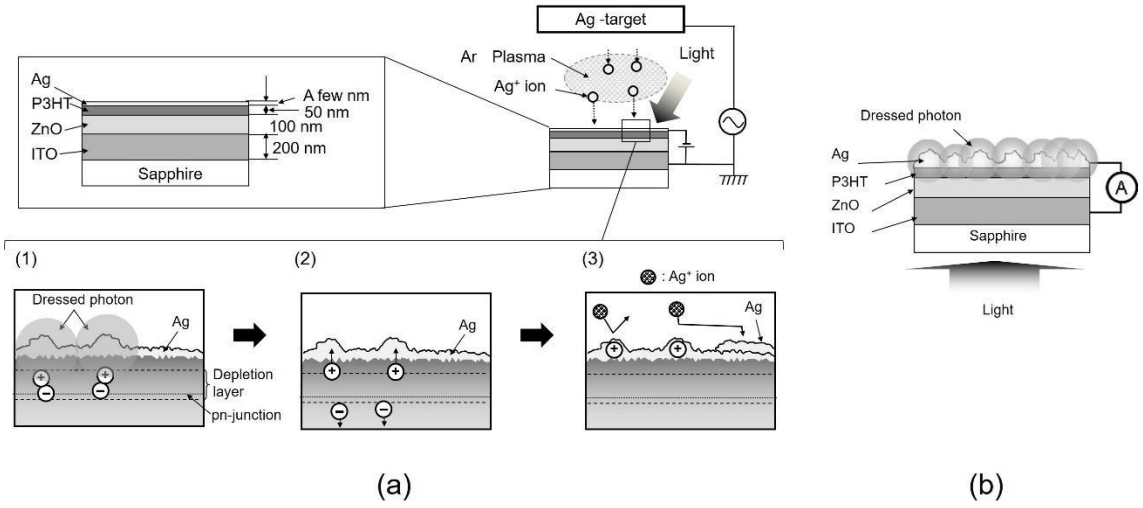

Fig. 11 Photovoltaic device using an organic P3HT film.

(a) Setup and method for autonomous fabrication. (1), (2), and (3) represent the creation of electron-hole pairs by the DP, charging the Ag film, and autonomous control of the Ag particle deposition, respectively. (b) Structure of the fabricated photovoltaic device.

Curve A in Fig. 12 represents the measured dependence of the generated photocurrent density on the wavelength of the incident light. For reference, curve B represents the photocurrent density that was generated from the device fabricated without rf-sputtering. It is confirmed that the values of curve A are much larger than those of curve B. Furthermore, the photocurrent was generated even though the wavelength of the incident light was longer than λ_c, experimentally confirming that the energy up-conversion above was achieved. The values of curve A take the maximum at

620 nm, which is nearly equal to λ_0 that indicates photon breeding*.

(*) The difference $\Delta\lambda$ between the peak wavelength of curve A and λ_0 originated from the DC Stark effect induced by the inverse voltage applied during the autonomous control of the surface of the Ag film.

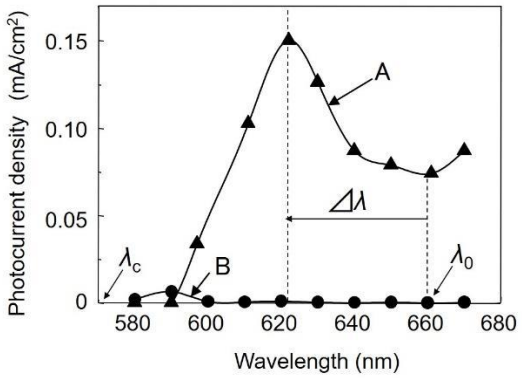

Fig. 12 Relation between the incident light wavelength and the photocurrent density. Curve A represents the measured results for the device fabricated by the present method. Curve B is for the device fabricated without rf-sputtering.

4 Comments for future theoretical approaches

Although the characteristics 1 and 2 in Section 3.1 have been reproduced by simulations based on the quantum master equations for the density matrices, their physical origins have never been analyzed. These origins were not discussed in a simulation of percolation either [10]. In view of such current situations in theoretical studies, novel theoretical models are required for propelling the analysis. In order to provide a clue to meet this requirement, experiments were carried out to evaluate the temporal behavior of the DP energy transfer among NPs. As a result, it was confirmed that this behavior was more prompt than that of the random-walk process [25]. This indicates that, to find the physical origins above and the origin of the autonomy in the

DP energy transfer, a novel theoretical model based on the quantum-walk theory may be more appropriate than one based on the random-walk theory.

5 Summary

By modifying the theoretical model based on on-shell science, size-dependent momentum resonance of DP energy transfer was described. A hierarchical feature was also described based on this resonance feature, and experimental evidence for it was presented. Next, the feature of autonomous DP energy transfer was reviewed and confirmed by experimental results obtained using DP devices, nano-fabrication, and energy conversion. It was pointed out that this feature was analogous to an intrinsic feature observed in organisms. Finally, to explore ways of analyzing this feature, it was pointed out that the use of the quantum-walk model is a promising theoretical tool.

References

[1] M. Ohtsu, I. Ojima, and H. Sakuma, *Progress in Opt*. **64** (Elsevier, 2019) pp.45-97.

[2] M. Ohtsu, *Dressed Photons*, (Springer, 2014) pp.11-88.

[3] M. Ohtsu, *Dressed Photons*, (Springer, 2014) pp.89-246.

[4] K. Kobayashi and M. Ohtsu, J.Microsc. 194, 249 (1999).

[5] S. Sangu, K. Kobayashi, and M. Ohtsu, J. Microsc. 202, 279 (2001).

[6] M. Naya, S. Mononobe, R. Uma Maheswari, T. Saiki, and M. Ohtsu, “Imaging of biological samples by a collection-mode photon scanning tunneling microscope with an aperture probe,” Opt. Commun. Vol.124 (1996) pp.9-15.

[7] N. Tate, M. Naruse, T. Yatsui, T. Kawazoe, M. Hoga, Y. Ohyagi, T. Fukuyama, M. Kitamura and M. Ohtsu, ”Nanophotonic code embedded in embossed hologram for hierarchical information retrieval,” *Optics Express*, **18**, 7497-7505 (2010).

[8] M. Ohtsu and T. Kawazoe, “Experimental estimation of the maximum size of a dressed photon,” Off-shell Archive (February 2018), Offshell:1802R.001.v1. **DOI**:10.14939/1802R.001.v1

[9] W. Nomura, T. Yatsui, T. Kawazoe, M. Naruse, and M. Ohtsu, Appl. Phys. B 100, 181 (2010).

[10] M. Naruse, S.J. Kim, T. Takahashi, M. Aono, K. Akahane, M. D’Acunto, H. Hori, L. Thylen, and M. Ohtsu, “Percolation of optical excitation mediated by near-field interactions,” Physica A, **471** (2017)pp.162-168.

[11] M. Ohtsu, T. Kawazoe, and H. Saigo, "Spatial and Temporal Evolutions of Dressed Photon Energy Transfer,”Off-shell Archive (October 2017),Offshell: 1710R.001.v1. **DOI**: 10.14939/1710R.001.v1

[12] M. Naruse, K. Leibnitz, F. Peper, N. Tate, W. Nomura, T. Kawazoe, M. Murata, M. Ohtsu, Nano Commun. Networks 2, 189 (2011).

[13] M. Naruse, T. Kawazoe, R. Ohta, W. Nomura, and M. Ohtsu, Phys. Rev. B 80, 125325 (2009).

[14] M. Aono, M. Naruse, S-J. Kim, M. Wakabayashi, H. Hori, M. Ohtsu, and M. Hara, “Amoeba-Inspired Nanoarchitectonic Computing: Solving Intractable Computational Problems Using Nanoscale Photoexcitation Transfer Dynamics,” Langmuir, Vol. 29, April 2013, pp. 7557-7564.

[15] M. Naruse, W. Nomura, M. Aono, M. Ohtsu, Y. Sonnefraud, A. Drezet, S. Huant, and S.-J Kim, “Decision making based on optical excitation transfer via near-field interactions between quantum dots,” J. Appl. Phys., Vol. 116 (2014) pp.154303-1～8.

[16] T. Yatsui, K. Hirata, W. Nomura, Y. Tabata, and M. Ohtsu, Appl. Phys. B 93, 55 (2008).

[17] T. Yatsui, K. Hirata, Y. Tabata, W. Nomura, T Kawazoe, M. Naruse, and M. Ohtsu, “*In situ* real-time monitoring of changes in the surface roughness during nonadiabatic optical near-field etching,” Nanotechnology, Vol. 21, No. 35, August 2010, pp. 355303 1-5.

[18] M. Ohtsu and T. Kawazoe, “Principles and Practices of Si Light Emitting Diodes

using Dressed Photons," Off-shell Archive (May 2018), Offshell:1805R.001.v1. **DOI**:10.14939/1805R.001.v1

[19] T. Kawazoe, M. A. Mueed, and M. Ohtsu, "Highly efficient and broadband Si homojunction structured near-infrared light emitting diodes based on the phonon-assisted optical near-field process," Appl. Phys. **B104**, 747 (2011).

[20] T. Kawazoe, K. Nishioka, and M. Ohtsu, Appl. Phys. **A 121**, 1409 (2015).

[21] M. Ohtsu, *Silicon Light-Emitting Diodes and Lasers* (Springer, 2016) pp.65-82.

[22] M. Ohtsu, *Silicon Light-Emitting Diodes and Lasers* (Springer, 2016) pp.83-101.

[23] M. Ohtsu, *Silicon Light-Emitting Diodes and Lasers* (Springer, 2016) pp.135-137.

[24] S. Yukutake, T. Kawazoe, T. Yatsui, W. Nomura, K. Kitamura, and M. Ohtsu, Appl. Phys. **B99**, 415 (2010).

[25] M. Ohtsu, T. Kawazoe, and H. Saigo, "Spatial and Temporal Evolutions of Dressed Photon Energy Transfer," Offshell:1710R.001.v1.